SUPPLEMENT TO THE *WELDING JOURNAL*, MAY 2022
Sponsored by the American Welding Society

Metallurgical Design Rules for High-Strength Steel Weld Metals

A dilatometric analysis of Fe-C-Mn high-strength steel weld metals offered metallurgical design rules for high-performance applications

BY K. SAMPATH

Abstract

A review of a dilatometric analysis of selected Fe-C-Mn high-strength steel shielded metal arc weld metals showed that balanced Ti, B, Al, O, and N additions reduced the austenite-to-ferrite transformation-start (T_s) temperature. These microalloy additions must match the following aim levels for composition control: Ti at 400 ppm (0.04 wt-%), B at 40 ppm (0.004 wt-%), Al at 200 ppm (0.020 wt-%), O at 400 ppm (0.04 wt-%), and N preferably below 80 ppm (0.008 wt-%) to ensure effective deoxidation, form complex inclusions, and distribute them to enable development of highly fracture-resistant refined weld metal microstructures. It may be wiser to avoid the rich and lean ends for these microalloy additions, except N, which should be held at the lean end, preferably much below 80 ppm (0.008 wt-%). The balanced Ti, B, Al, O, and N additions offered nearly a 100°C shift in lowering the Charpy V-notch (CVN) test temperature for either 28 or 100 J absorbed energy. Dilatometric evaluations of reheated weld metals showed that 1) the balanced Ti, B, Al, O, and N additions lowered the actual T_s temperature by about 60°C compared to the calculated austenite-to-ferrite transformation temperature obtained from the constitutional equation; 2) N with more than 100 ppm (0.010 wt-%) effectively nullified the beneficial effects of Ti, B, and Al additions in lowering the transformation temperature; and 3) at N content much below 80 ppm (0.008 wt-%), both a lower T_s temperature and a narrow start-to-finish (T_s–T_f) temperature range helped in achieving exceptional weld metal CVN impact toughness.

https://doi.org/10.29391/2022.101.010

Keywords

- Fe-C-Mn High-Strength Steels
- SMAW
- Database
- Electrode Development
- Calculated Metallurgical Characteristics
- Dilatometry
- Weld Mechanical Properties
- Metallurgical Design Rules

Introduction

It is well known that carbon content has the utmost adverse effect on the weldability of Fe-C-Mn high-strength steels (Ref. 1). Here, one could define weldability, in terms of microstructure development and/or control, as the ability of the selected welding process and conditions to eliminate defects while recreating a high-performance microstructure similar to the base metal in the fusion zone and retaining the high-performance base metal microstructure in the heat-affected zone (HAZ) for ensuring high weld joint efficiency and exceptional fracture toughness. Commonly, joint efficiency is expressed as a ratio of weld metal (WM) tensile strength to base metal tensile strength. In welded construction, a joint efficiency higher than 100% is usually preferred.

The weldability of Fe-C-Mn high-strength steels is often related to carbon content and the occurrence of martensite containing microstructures that have a higher sensitivity to cause hydrogen-assisted cracking (HAC). When the carbon content exceeds 0.12 wt-%, the morphology of martensite is likely to change from laths to plates, and this change in morphology more adversely affects cracking sensitivity when certain other conditions also simultaneously prevail. These other conditions include 1) a source of dissolved hydrogen; 2) high-residual tensile stress distribution; 3) a temperature range that did not allow significant solid-state diffusion of

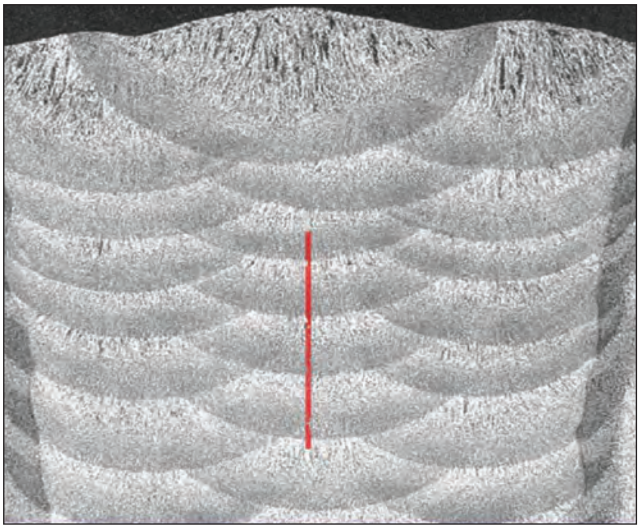

Fig. 1 — Cross section of a typical test weldment with three beads per layer (Ref. 23).

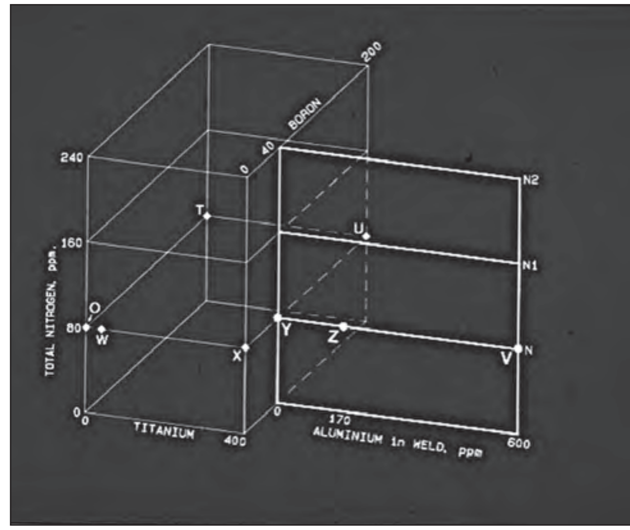

Fig. 2 — Basic scheme used in building a TiBAlN series of SMA welds (Ref. 25).

atomic hydrogen from the weldment; and 4) a time delay following welding that allowed atomic hydrogen to accumulate at internal flaws in the weldment. In view of this, base metal dilution during fusion welding requires consideration, and it is preferable to limit electrode carbon content to 0.10 wt-% or less.

Several research studies have evaluated the effects of various alloying elements, including C (Ref. 2), on microstructure development and the resultant mechanical properties of high-strength steel WMs. Such studies varied primarily one or a few alloy element(s) at a time, and these alloy elements included Mn (Ref. 3), Si (Ref. 4), Mo (Ref. 5), microalloy additions (Ref. 6), Al and Ti (Ref. 7), Ti and B (Ref. 8), etc., over a broader range and identified the minimum and maximum levels of the element(s) in meeting or exceeding specific WM microstructure and/or weld mechanical property requirements. These studies often provide insightful metallurgical background in understanding possible underlying mechanisms that facilitate the development of certain WM microstructures.

However, in multicomponent Fe-C-Mn systems, the interactive effects of various alloy elements could likely undermine the effective operation of one or more such mechanisms and might not allow one to achieve the anticipated benefits in meeting or exceeding mechanical property requirements; for example, when thermodynamically feasible and kinetically favorable Nb (Cb), Ti, V, Mo, W, Cr, and Mn alloy additions form carbides in decreasing order and thereby reduce carbon in solution, thus significantly decreasing the adverse effect of carbon on sensitivity to HAC.

Under this context, the following metallurgical principle on Fe-C-Mn high-strength steels might make enormous sense: Lowering the austenite decomposition (i.e., relevant solid-state phase transformation) temperatures improves both WM strength and fracture toughness, while simultaneously reducing both carbon content and carbon equivalency, improves weldability. Lowering the solid-state phase transformation temperatures is known to refine matrix grain size and simultaneously improve both strength and toughness.

The welding literature offers several constitutive equations to calculate carbon equivalency and estimate the weldability of various types of high-strength steels, primarily to evaluate their sensitivity to HAC and to select conditions and parameters for enforcing appropriate low-hydrogen fusion welding practices. In this regard, the following are three widely used constitutive equations:

$$P_{cm} = C + Si/30 + (Mn + Cu + Cr)/20 + Ni/60 + Mo/15 + V/10 + (5 \times B) \quad (1)$$

developed by Ito and Bessyo (Ref. 9) primarily for pipeline steels.

$$CE_{IIW} = C + (Mn + Si)/6 + (Cr + Mo + V)/5 + (Ni + Cu)/15 \quad (2)$$

used for a variety of structural steels. The above equation is a simplified form of Dearden and O'Neill's original formula for hardenability (Ref. 10) that was subsequently adopted by the International Institute for Welding (IIW) in 1967 and became a generally accepted measure of steel weldability.

The carbon equivalent number (CEN) developed by Yurioka, Suzuki, Ohshita, and Saito (Ref. 11) is used for various types of modern structural, pipeline, and pressure vessel steels:

$$CEN = C + \{A(C) \times EMU\} \quad (3)$$

where A(C) refers to the accommodation factor that is a function of the C content, while EMU refers to a set of elemental multiplication units involving Si, Mn, Cu, Ni, Cr, Mo, V, Nb (Cb), and B:

$$A(C) = 0.75 + 0.25 \tanh [20 \times (C - 0.12)] \quad (4)$$

Table 1 — Chemical Composition of 13 TiBAlN Series Welds (Refs. 21, 22)

Weld ID	Weld Metal Chemical Composition (wt-%)								
	C	Mn	P	S	Si	Cr	Ni	Mo	V
O	0.074	1.4	0.007	0.008	0.25	0.03	0.03	0.005	0.0005
O2	0.073	1.66	0.008	0.009	0.27	0.03	0.03	0.005	0.0005
X	0.069	1.47	0.006	0.005	0.45	0.03	0.03	0.005	0.0005
X2	0.068	1.46	0.006	0.007	0.47	0.03	0.03	0.005	0.0005
Y	0.07	1.57	0.01	0.006	0.45	0.03	0.03	0.005	0.0005
Y2	0.069	1.51	0.008	0.007	0.36	0.03	0.03	0.005	0.0005
Z	0.072	1.56	0.01	0.007	0.49	0.03	0.03	0.005	0.0005
Z2	0.068	1.45	0.011	0.006	0.5	0.03	0.03	0.005	0.0005
U	0.073	1.52	0.011	0.006	0.4	0.03	0.03	0.005	0.0005
U2	0.066	1.4	0.012	0.007	0.36	0.03	0.03	0.005	0.0005
V	0.078	1.44	0.007	0.006	0.6	0.03	0.03	0.005	0.0005
V1	0.067	1.44	0.01	0.005	0.63	0.03	0.03	0.005	0.0005
V2	0.069	1.42	0.012	0.006	0.6	0.03	0.03	0.005	0.0005
Low	0.066	1.4	0.006	0.005	0.25	0.03	0.03	0.005	0.0005
High	0.078	1.66	0.012	0.009	0.63	0.03	0.03	0.005	0.0005
Range	0.012	0.26	0.006	0.004	0.38	0	0	0	0

and

$$\mathrm{EMU} = \{\mathrm{Si}/24 + \mathrm{Mn}/6 + \mathrm{Cu}/15 + \mathrm{Ni}/20 + (\mathrm{Cr} + \mathrm{Mo} + \mathrm{V} + \mathrm{Nb})/5 + 5 \times \mathrm{B}\} \quad (5)$$

The above constitutive equations include microalloy additions such as V, Nb (Cb), and B, besides various principal alloy elements such as C, Mn, Cr, Ni, Mo, and Cu.

How does one lower the austenite decomposition temperature? In general, there are two means available: 1) through proper control of (electrode and WM) chemical composition, and 2) by increasing the (weld) cooling rate that enables undercooling. The following constitutive (statistical/regression) equations relate various austenite decomposition temperatures, such as austenite-to-ferrite (A_{r3}) (Ref. 12), bainite-start (B_S), 50% bainite (B_{50}), bainite-finish (B_f), and martensite-start (M_S) (Ref. 13), with the contents of principal alloy elements:

$$A_{r3}\ (^\circ\mathrm{C}) = 910 - (310 \times \mathrm{C}) - (80 \times \mathrm{Mn}) - (80 \times \mathrm{Mo}) - (55 \times \mathrm{Ni}) - (20 \times \mathrm{Cu}) - (15 \times \mathrm{Cr}) \quad (6)$$

Table 1 — (continued)

Weld ID	Weld Metal Chemical Composition (wt-%)						
	Nb	Cu	Ti	B	O	Al	N
O	0.0005	0.03	0.0001	0.0001	0.0475	0.0006	0.0079
O2	0.0005	0.03	0.0005	0.0005	0.0399	0.0005	0.0235
X	0.0005	0.03	0.041	0.0002	0.0282	0.0001	0.0077
X2	0.0005	0.03	0.045	0.0002	0.0297	0.0005	0.0249
Y	0.0005	0.03	0.039	0.0039	0.0308	0.0013	0.0083
Y2	0.0005	0.03	0.041	0.0044	0.0292	0.0005	0.0232
Z	0.0005	0.03	0.042	0.0048	0.0438	0.016	0.0067
Z2	0.0005	0.03	0.047	0.0045	0.044	0.018	0.023
U	0.0005	0.03	0.039	0.0158	0.029	0.0005	0.0084
U2	0.0005	0.03	0.039	0.0167	0.0297	0.0005	0.0217
V	0.0005	0.03	0.054	0.0056	0.044	0.058	0.0041
V1	0.0005	0.03	0.048	0.0044	0.0473	0.056	0.012
V2	0.0005	0.03	0.043	0.0035	0.047	0.056	0.0235
Low	0.0005	0.03	0.0001	0.0001	0.0282	0.0001	0.0041
High	0.0005	0.03	0.054	0.0167	0.0475	0.058	0.0249
Range	0	0	0.0539	0.0166	0.0193	0.0579	0.0208

$$B_s\,(°C) = 830 - (270 \times C) - (90 \times Mn) - (37 \times Ni) - (70 \times Cr) - (83 \times Mo) \quad (7)$$

$$B_{50}\,(°C) = 770 - (270 \times C) - (90 \times Mn) - (37 \times Ni) - (70 \times Cr) - (83 \times Mo) \quad (8)$$

$$B_f\,(°C) = 710 - (270 \times C) - (90 \times Mn) - (37 \times Ni) - (70 \times Cr) - (83 \times Mo) \quad (9)$$

$$M_s\,(°C) = 561 - (474 \times C) - (33 \times Mn) - (17 \times Ni) - (17 \times Cr) - (21 \times Mo) \quad (10)$$

As shown, the calculated B_s and B_f temperatures differ by 120°C, and the B_{50} temperature is midway between the calculated B_s and B_f temperatures. Equations 6–10 indicate that all principal alloy elements decrease austenite decomposition temperatures with carbon affecting to a maximum extent, particularly when carbon content exceeds 0.12 wt-%. These equations were developed several decades ago and can be used to calculate or estimate the transformation temperatures when the cooling rate supposedly remains constant. However, these constitutive equations for transformation temperatures make no reference to Ti-B-Al-O-N additions. Modern high-strength steels, such as HSLA-65 (Ref. 14), contain various microalloy additions, such as Ti, V, and Nb (Cb). Therefore, application of the above constitutive equations to calculate austenite transformation temperatures of modern steels offers only approximations of actual values.

Metallurgical Design of Welding Electrodes

Over the past three decades, the set of constitutive equations have been successfully used to metallurgically design the contents of principal alloy elements in welding electrode and WM compositions of higher strength steels (Refs. 15, 16). As mentioned earlier, the intrinsic effect of carbon on the weldability of steels is well known. Similarly, the trends on the interactive effects of other elements on weldability, microstructure development, strength, and fracture toughness are also well known. However, these trends are difficult to quantify in terms of desired or acceptable values for WM strength and Charpy V-notch (CVN) impact toughness, particularly when applied to a variety of high-strength Fe-C-Mn steels and over a broad range of weld heat input or weld cooling rates.

For example, AWS A5.1, *Specification for Carbon Steel Electrodes for Shielded Metal Arc Welding*, lists or tabulates classification requirements of WM composition and mechanical properties. Here, mechanical property test results generated using a fixed or standardized welding procedure involving joint geometry, heat input, bead sequence, etc., can be considered desirable baselines to adequately characterize a composition of a particular electrode's covering (or basicity index). The basicity index is commonly used to characterize fluxes. Discussions of shielded metal arc welding (SMAW) electrode design normally emphasize the importance of the electrode covering and resultant slag composition, a consequence of various chemicals in the electrode covering and their interactions in the molten weld pool. This specific characterization is important to WM deposit composition, cleanliness (i.e., amount and size distribution of inclusions), and ultimately to WM microstructure and mechanical properties. When the flux system changes, the basicity might change, and the WM composition might also change, thereby affecting the resultant WM mechanical properties.

Similarly, for diffusion-controlled phase transformations, the cooling rate is expected to control the development of the type and size of various microstructural constituents, thus affecting the characteristics of the WM. Changing the welding heat input/arc energy or the electrode diameter will change the times and temperatures available for diffusion-controlled transformations, thus affecting the resultant WM composition.

Depending on the specific weld procedure used, the reheat zones can be aligned, or the amount of as-deposited WM can be maximized, and the expected mechanical properties can vary just based on the WM microstructure being sampled.

To this end, the University of Cambridge performed a neural network analysis of a vast and fairly general database assembled from publications on WM properties involving yield strength, ultimate tensile strength (UTS) (Ref. 17), elongation, and Charpy impact toughness (Ref. 18) of ferritic steel WM expressed as functions of chemical composition, heat input during welding, and postweld heat treatment. The outputs

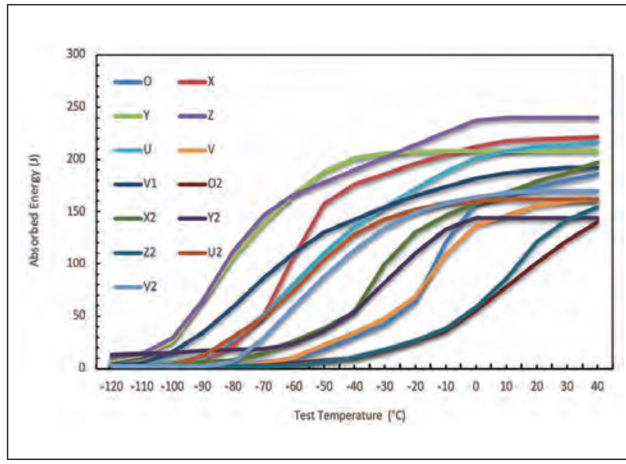

Fig. 3 — CVN absorbed energy values of TiBAlN series of welds against test temperatures (Ref. 25).

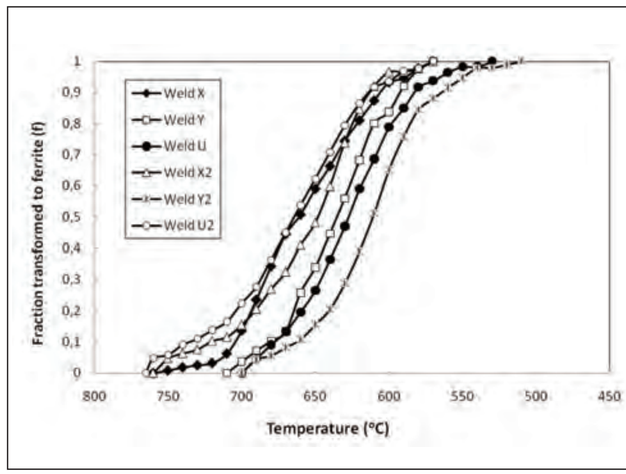

Fig. 4 — Dilatometric evaluation of austenite-to-ferrite transformation (Ref. 26).

of the model were assessed in a variety of ways, including specific studies of model predictions for the Fe-C-Mn and Fe-2.25Cr-1Mo systems. Comparisons were also made with corresponding methods, which use simple physical metallurgical principles. The models appeared to capture vital metallurgical trends and emulate expectations from current physical metallurgy principles yet required much more systematic experimental data to improve the accuracy of their predictions.

The U.S. Navy used a neural network technique due to MacKay with a Bayesian framework wherein the probability (of occurrence) is interpreted as a reasonable expectation of a state of current knowledge but allows estimation of error bars and warns the user when data is sparse or locally noisy. This neural network was trained and tested on a set of data obtained on WMs on types of steels used for shipbuilding (Ref. 19). The input variables for the network used WM chemical composition and weld cooling rate. The outputs consisted of yield and UTSs, elongation, and reduction of area. This effort created many models using different network configurations and initial conditions. The method revealed

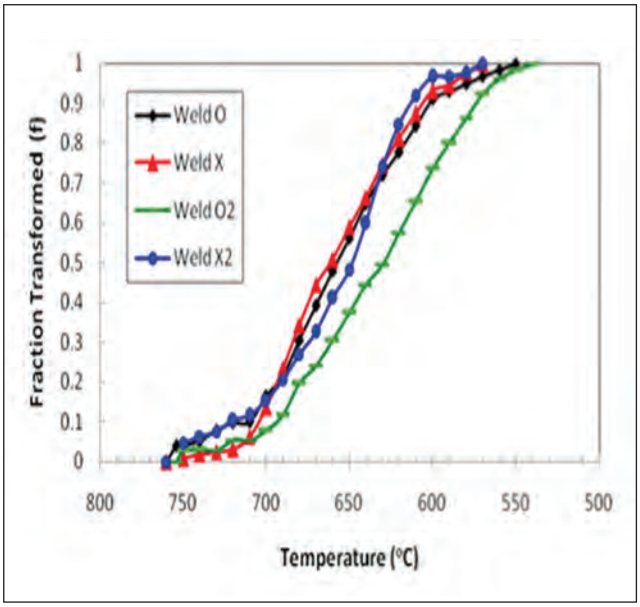

Fig. 5 — Dilatometric evaluation of austenite-to-ferrite transformation (Ref. 27).

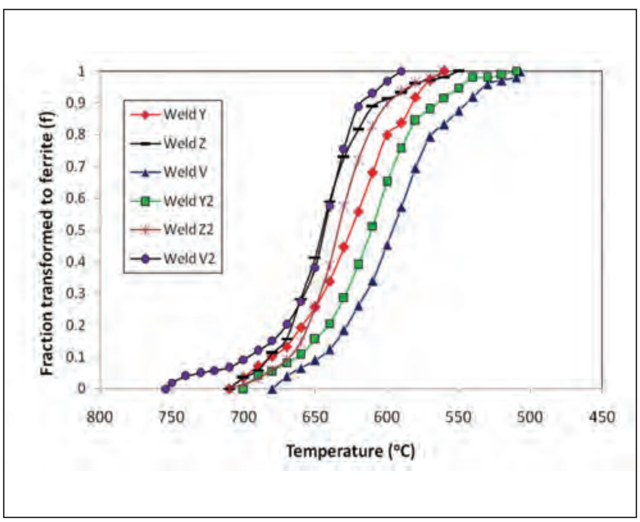

Fig. 6 — Dilatometric evaluation of austenite-to-ferrite transformation (Ref. 28).

significant trends describing the dependence of mechanical properties on weld composition and cooling rate. The U.S. Navy also used a similar approach to model WM toughness characterized by CVN and dynamic tear tests of the same types of steels (Ref. 20). The level of noise in the experimental data was perceived to be high, but it nevertheless allowed one to recognize reasonable trends and uncertainties when making predictions. For example, the WM toughness showed a nonlinear deterioration as the WM oxygen concentration increased, yet this behavior could be assessed quantitatively.

The above complexities involving a variety of variables and uncertainties affect near-accurate predictions of WM strength and toughness from neural network modeling based on WM chemical composition and weld cooling rate. Instead, welding electrode designers could simply capture known trends in terms of certain calculated metallurgical characteristics (CMCs) and box the desired values for the various CMCs in selected numerical ranges, thereby allowing one to obtain desirable WM microstructures and resultant mechanical properties that exceed the minimum specified requirements. The boxing also enables one to achieve an adequate buffer to accommodate the effects of variations in weld heat input and the associated range of weld cooling rates on a desirable range for weld mechanical properties.

The desired WM microstructure could be predominantly either diffusional transformation products, such as acicular ferrite when the desired WM strength is 700 MPa (N/mm^2) or about 100 ksi, or displacive (athermal) transformation products, such as bainite and/or martensite, when the desired WM strength is much more than 700 MPa or 100 ksi. In this continuum, indiscriminate lowering of solid-state phase transformation temperatures through excessive additions of Mn, Ni, or Mo could result in violation of the common progression of transformation temperatures, wherein $A_{r3} > B_s > B_f > M_s$, and lead to adverse consequences, particularly on WM toughness when diffusional transformation products are desired in the WM microstructure. When athermal transformation products are desired in the WM microstructure, one could consider suitably manipulating the differences among the calculated values of $B_s–M_s$, $B_{50}–M_s$, or $B_f–M_s$ temperatures (Ref. 15).

In addition to the type and amount of principal alloy elements, welding electrode designers are also concerned with the type and amount of other alloy elements, such as S, P, Si, Nb (Cb), V, Ti, Al, Zr, B, etc. The control of these other elements and the total gas (hydrogen, oxygen, and nitrogen) content is critical to eliminating weld defects and promoting desirable combinations in WM microstructure development. Depending on their nominal content and actual effects during welding and/or following postsoak heat treatment, these other elements either enhance or impair WM soundness, cleanliness, and mechanical properties, particularly fracture toughness or low-temperature CVN impact toughness.

Evans' SMAW Database

Over the years, a large database containing more than 900 Fe-C-Mn high-strength steel SMA WM compositions was developed at Oerlikon Welding Ltd., Zurich, Switzerland (Refs. 21, 22). This database includes a complete listing of WM compositions, all-weld tensile properties at ambient temperature, and WM CVN impact toughness test results. In particular, the CVN impact properties list the test temperature that achieved 28 and 100 J impact energy for each WM composition. The CVN impact toughness of selected welds were also obtained over a temperature range of –120° to +40°C. Availability of this large SMAW database is a valuable and rare gift to the welding community, as it provides ready access to a wealth of data.

The various experimental SMAW electrodes mostly belonged to the basic type. The test weld deposits were produced using standardized procedures at Oerlikon Welding Ltd., according to ISO 2560 — *Welding Consumables — Covered Electrodes for Manual Metal Arc Welding of Non-Alloy and Fine Grain Steels — Classification*, at a heat-input

Table 2 — Tensile and CVN Impact Properties of 13 TiBAlN Series Welds (Refs. 21, 22)

Weld ID	Weld Metal Tensile Properties				CVN Test Temperature (°C)	
	YS (MPa)	UTS (MPa)	El (%)	RA (%)	@ 100 J	@ 28 J
O	445	528	28	78	–14	–42
O2	505	607	24	76	20	–16
X	504	577	26	80	–61	–77
X2	578	631	25	78	–30	–58
Y	546	594	25.8	73.0	–82	–98
Y2	539	605	23.9	71.6	–24	–56
Z	610	640	27.2	73.4	–83	–100
Z2	493	583	26.8	69.2	13	–18
U	517	586	23	78	–53	–80
U2	474	541	28	73	–52	–81
V	668	732	20.3	69.7	–12	–46
V1	571	644	25	74	–64	–93
V2	529	591	25.6	73.8	–45	–70
Low	445	528	20.3	69.2	–83	–100
High	668	732	28	80	20	–16
Range	223	204	7.7	10.8	103	84

of 1 kJ/mm, 200°C interpass temperature and 20 mm plate thickness by a single master welder. Figure 1 shows a typical macrograph of a test weld (Ref. 23), the CVN being centrally located as shown by the vertical red line, as specified in standards.

A recent publication on the analysis of this high-strength steel SMAW database (*aws.org/2021.100.036-database*) offered a constraints-based model (CBM) as a simple framework to effectively organize and analyze the database in gaining valuable insights (Ref. 24). The constraints refer to a selection of numerical ranges for the CEN and calculated solid-state phase transformation temperatures related to the decomposition of austenite, such as A_{r3}, B_S, B_f, and M_S temperatures. The CBM identifies a set of constitutive equations, calculates their numerical values, and simultaneously solves them in a mutually inclusive fashion to meet certain numerical ranges for chemical composition and specific metallurgical characteristics of interest. In other words, the CBM employs a mathematical approach to address specific metallurgical needs, in which the outcome of each decision is constrained by minimum and maximum limits as detailed in the boundary conditions for various elements and CMCs. Decision variables, such as CEN, B_S, B_f, M_S, etc., that share a common constraint,

Table 3 — Selected CMCs of 13 TiBAlN Series Welds

Weld ID	Selected Calculated Metallurgical Characteristics											
	P_{cm}	CE_{IIW}	CEN	A_{r3} (°C)	B_S (°C)	B_{50} (°C)	B_f (°C)	M_S (°C)	$(B_f–M_S)$ (°C)	$(A_{r3}–B_S)$ (°C)	$(A_{r3}–B_{50})$ (°C)	$(A_{r3}–B_f)$ (°C)
O	0.157	0.360	0.219	772	680	620	560	479	82	92	152	212
O2	0.162	0.406	0.243	751	657	597	537	470	67	94	154	214
X	0.187	0.400	0.223	768	675	615	555	479	77	92	152	212
X2	0.194	0.401	0.221	769	677	617	557	479	77	92	152	212
Y	0.245	0.418	0.244	760	666	606	546	475	71	93	153	213
Y2	0.202	0.392	0.236	765	672	612	552	477	75	93	153	213
Z	0.186	0.425	0.250	760	667	607	547	474	72	93	153	213
Z2	0.171	0.404	0.232	770	678	618	558	480	78	92	152	212
U	0.162	0.404	0.277	763	670	610	550	475	75	93	153	213
U2	0.182	0.370	0.255	774	683	623	563	482	80	92	152	212
V	0.184	0.429	0.254	768	676	616	556	475	80	92	152	212
V1	0.235	0.423	0.232	771	679	619	559	481	78	92	152	212
V2	0.181	0.417	0.231	772	680	620	560	480	80	92	152	212
Low	0.157	0.36	0.219	751	657	597	537	470	67	92	152	212
High	0.245	0.429	0.277	774	683	623	563	482	82	94	154	214
Range	0.088	0.069	0.058	23	26	26	26	12	15	2	2	2

such as a specified chemical composition range for principal alloy elements, must also have their solution values fall within the bounds of the various constraints.

Analysis of this large SMAW database, using the CBM as a framework, reaffirmed that controlling carbon content, the value of CEN, and calculated solid-state phase transformation temperatures, particularly the difference between the calculated B_S and M_S temperatures, is critical to developing and identifying high-performance, high-strength steel welding electrodes and WMs.

Ti-B-Al-O-N Additions

A part of Evans' large SMAW database used a separate or an independent scheme to build a total of 24 SMA welds based on a TiBAlN series (Ref. 25). These 24 welds included a set of eight welds, each at three levels of nitrogen content — normal (below 85 ppm or 0.0085 wt-%), intermediate (120 to 164 ppm or 0.012 to 0.0164 wt-%), and high (217 to 249 ppm or 0.0217 to 0.0249 wt-%). The primary intent of this subset of WMs was to identify and correlate the effects of Ti-B-Al-O-N alloy additions on WM tensile strength, CVN

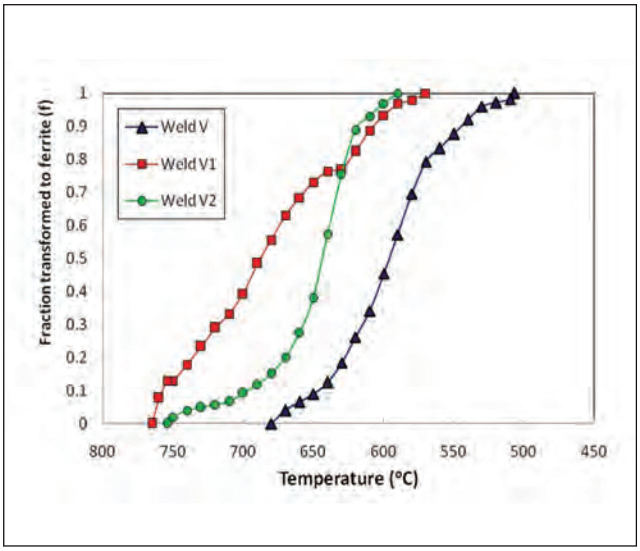

Fig. 7 — Dilatometric evaluation of austenite-to-ferrite transformation (Ref. 28).

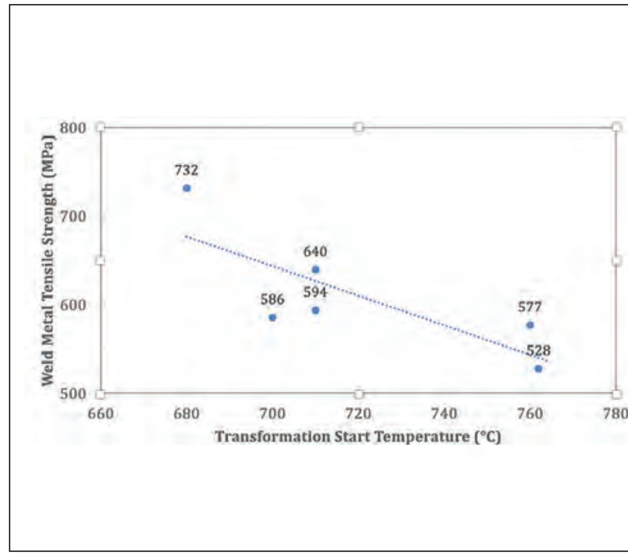

Fig. 8 — Effect of transformation start temperature on WM tensile strength.

impact toughness, and microstructure development in the fusion zone and reheated WM.

The first set of eight welds with the lowest or normal nitrogen content at less than 85 ppm or 0.0085 wt-% are named O, W, X, Y, Z, T, U, and V. These are shown in a grid pattern illustrated in Fig. 2. The grid pattern shows Ti and Al additions along the X-axis, N addition along the Y-axis, and B addition along the Z-axis.

At first, Ti alone was added to O to give W (at 28 ppm or 0.0028 wt-% Ti) and X (at 410 ppm or 0.041 wt-% Ti). Then B was added to produce Y (at 39 ppm or 0.0039 wt-% B), and Al was added to give Z (at 160 ppm or 0.016 wt-% Al). Also, excess B and Al were added to generate welds T, U, and V at the far extremes.

The second set of eight WMs with an intermediate nitrogen content in the 120 to 164 ppm or 0.012 to 0.0164 wt-% range are named O1, W1, X1, Y1, Z1, T1, U1, and V1. The third set of eight WMs with a much higher N content in the 217 to 249 ppm or 0.0217 to 0.0249 wt-% range are named O2, W2, X2, Y2, Z2, T2, U2, and V2.

Table 1 shows the chemical composition of 13 of 24 TiBAlN series of SMA WMs (Refs. 21, 22). The C content of these 13 WMs varied between 0.066 and 0.078 wt-%, while the Mn content varied between 1.4 and 1.66 wt-% and Si content varied between 0.25 and 0.63 wt-%. Other principal alloy elements remained constant: Cr content at 0.03 wt-%, Ni content at 0.03 wt-%, Mo content at 0.005 wt-%, and Cu content at 0.03 wt-%. Compared to the principal alloy elements, Ti content varied between 0.0001 and 0.054 wt-%, B content ranged between 0.0001 and 0.0167 wt-%, O content varied between 0.0282 and 0.0475 wt-%, Al content varied between 0.0001 and 0.058 wt-%, and N content varied between 0.0041 and 0.0249 wt-%.

Following weld mechanical testing that included all-WM tensile testing at ambient temperature, and CVN impact testing over a wider temperature range from –120 to +40°C, these 13 WMs were subjected to dilatometric evaluation (Refs. 26–28). These 13 WMs, as shown in Table 1, were selected to allow dilatometric evaluation of specific alloy additions relative to a range of Ti, B, Al, O, and N contents, particularly the effect of nitrogen content at three levels on both transformation-start (T_s) and transformation-finish (T_f) temperatures. The dilatometric evaluation studied the A_{r3} transformation during continuous cooling. Test specimens were machined to form hollow cylinders with the following dimensions: 10 mm long × 5 mm outside diameter with 1 mm wall thickness. The axis of the test specimen was maintained parallel to the original welding direction. The specimens were subjected to the following controlled thermal cycle: austenitization at 1250°C for two minutes followed by continuous cooling at a typical (weld) cooling rate of 13°C/s from 800° to 500°C.

The study determined the T_s, 50% transformation (T_{50}), peak rate transformation (T_{PRTT}), and T_f temperatures of the 13 (O, O2, X, X2, Y, Y2, Z, Z2, U, U2, V, V1, and V2) welds. These 13 welds contained Ti content between 1 (0.0001) and 54 ppm (0.0054 wt-%) and B content between 1 (0.0001) and 167 ppm (0.0167 wt-%).

Objectives

The purpose of this review is to do the following:

1) Obtain the CMCs of 13 Fe-C-Mn SMAWs containing various Ti-B-Al-O-N additions using selected constitutive equations, and compare the calculated A_{r3} temperature with the T_s temperature determined using dilatometry;

2) Calculate and predict the temperature for 28 J CVN impact toughness or the absorbed energy of 13 WMs using neural network analysis available through The Japan Welding Engineering Society (JWES) website (*www-it.jwes.or.jp/weld_simulator/en/cal6.jsp*);

3) Use the above results to provide an understanding of the effects of Ti-B-Al-O-N additions on microstructure development and to identify a few metallurgical rules for

Table 4 — Absorbed Energy of Charpy V-Notch Tests of 13 TiBAlN Series Welds (Ref. 25)

Weld ID	Absorbed Energy (Joules) at Test Temperatures (°C)								
	–120	–110	–100	–90	–80	–70	–60	–50	–40
O	2	2	2	2	3	6	9	18	30
O2	2	2	2	2	2	3	5	8	10
X	3	4	5	8	22	50	107	157	176
X2	2	2	3	6	8	14	26	38	54
Y	8	13	26	65	106	138	166	188	201
Y2	13	14	15	17	18	19	24	36	54
Z	10	14	29	65	112	146	166	178	190
Z2	2	2	2	2	2	2	3	7	11
U	3	4	6	10	28	51	81	110	136
U2	2	2	4	12	30	49	74	104	128
V	2	2	2	2	2	5	11	23	34
V1	2	5	16	34	59	86	110	130	142
V2	2	2	2	2	6	29	59	88	113

designing the chemical composition of high-strength, high-performance steel welding electrodes; and

4) Perform validation testing to further ascertain the validity of the metallurgical rules for designing high-strength, high-performance steel welding electrodes when the results of dilatometric evaluations were not available.

Procedure

The current effort used the Evans' SMA Fe-C-Mn WM chemical composition database and obtained the CMCs using previously cited constitutive (statistical/regression) equations, Equations 1–10.

These constitutive equations relate austenite transformation temperatures to the contents of principal alloy elements like C, Mn, Ni, Cr, Mo, and Cu, but do not include the effects of various minor alloy elements like Al, O, N, and particularly Ti and B. Consequently, one shouldn't expect that the calculated austenite transformation temperatures would fully agree with the dilatometric experimental results of solid-state phase transformation temperatures, more so as they relate to WMs.

The values of various CMCs were obtained using Microsoft Excel. Subsequently, the results were transposed (i.e., organized) to perform a variety of comparative analyses. The Microsoft Excel Workbook, TiBAlN SMAW Database, available on the AWS website (*aws.org/2022.101.010-database*) contains a total of six spreadsheets. Spreadsheet #1 contains Evans' original database together with various CMCs, and Spreadsheet #2 shows the 24 TiBAlON WM compositions that included the three sets of eight welds, each at three levels of nitrogen — normal, intermediate, and high. Spreadsheet #3 shows the 13 TiBAlON WM compositions that were used in subsequent dilatometric evaluations.

Spreadsheets #4–#6 provide the results of additional validation testing when the results of dilatometric evaluations of related WMs were not available. The validation testing used –100°C (Spreadsheet #4), –68°C (Spreadsheet #5), and –92°C (Spreadsheet #6) temperatures as the cutoff for

Table 4 — (continued)

Weld ID	Absorbed Energy (Joules) at Test Temperatures (°C)							
	–30	–20	–10	0	10	20	30	40
O	42	64	121	158	166	174	180	186
O2	17	26	36	56	78	101	122	140
X	186	196	204	212	218	219	220	221
X2	100	130	146	158	168	179	187	197
Y	206	207	208	208	208	208	208	208
Y2	82	110	133	144	144	144	144	144
Z	202	214	226	237	240	240	240	240
Z2	18	27	38	59	86	121	142	154
U	154	172	188	201	208	212	214	216
U2	143	152	158	160	162	162	162	162
V	48	69	109	137	146	156	160	162
V1	154	165	174	182	187	190	192	192
V2	134	149	158	164	168	170	170	170

28 J CVN impact toughness or absorbed energy to identify the respective WMs and their range of CMCs.

The 13 TiBAlN WM chemical composition data were also used to obtain and thus ascertain the temperature for 28 J CVN impact toughness or absorbed energy. The JWES website provides the required template to perform these predictive calculations based on the chemical composition of Fe-C-Mn WMs with certain minimum and maximum limits for specific elements.

Results

Effects of Ti-B-Al-O-N Additions

Table 2 shows the tensile and CVN impact properties of the 13 TiBAlN series welds (Refs. 21, 22). In particular, the CVN impact properties show the test temperatures that achieved 100 and 28 J absorbed energy. The 13 welds showed the test temperatures for 100 J absorbed energy varied from –83° to +13°C, while the test temperatures for 28 J absorbed energy varied from –100° to –16°C.

Weld O showed the lowest UTS at 528 MPa (Table 2), consistent with its low alloy content (Table 1). Weld V showed the highest UTS at 732 MPa. Weld V showed a low N content at 41 ppm (0.0041 wt-%) but excessive amounts of Ti content at 540 ppm (0.054 wt-%), B content at 56 ppm (0.0056 wt-%), O content at 440 ppm (0.044 wt-%), and Al content at 580 ppm (0.058 wt-%). Weld V1 showed the second highest UTS at 644 MPa, followed by weld Z, which showed 640 MPa UTS. Additionally, weld Z showed the best (i.e., lowest) CVN toughness test temperatures for both 100 and 28 J absorbed energy. A comparison of Z2 and Z welds revealed the CVN test temperature for 100 J absorbed energy lowered from 13° to –83°C, while that for 28 J absorbed energy lowered from –18° to –100°C, causing almost a –100°C transition. The superior CVN impact toughness behavior of weld Z occurred

Table 5 — Test Results of Transformation Temperature of 13 TiBAlN Welds at 13°C/s Cooling Rate (Refs. 26–28)

Weld ID	Ti Content (wt-%)	B Content (wt-%)	N Content (wt-%)	UTS (MPa)	CVN Test Temperature (°C)		Transformation Temperature (°C)				
					@ 100 J	@ 28 J	T_S	T_{50}	T_{PRTT}	T_f	$(T_S–T_f)$
O	0.0001	0.0001	0.0079	528	–14	–42	762	658	650	554	208
O2	0.0005	0.0005	0.0235	607	20	–16	754	630	606	534	220
X	0.041	0.0002	0.0077	577	–61	–77	760	660	630	568	192
X2	0.045	0.0002	0.0249	631	–30	–58	760	650	638	572	188
Y	0.039	0.0039	0.0083	594	–82	–98	710	625	618	560	150
Y2	0.041	0.0044	0.0232	605	–24	–56	703	612	606	510	193
Z	0.042	0.0048	0.0067	640	–83	–100	710	645	642	550	160
Z2	0.047	0.0045	0.023	583	13	–18	703	635	632	560	143
U	0.039	0.0158	0.0084	586	–53	–80	700	626	620	531	169
U2	0.039	0.0167	0.0217	541	–52	–81	765	662	650	574	191
V	0.054	0.0056	0.0041	732	–12	–46	680	598	596	507	173
V1*	0.048	0.0044	0.012	644	–64	–93	760	680	640	555	205
V2	0.043	0.0035	0.0235	591	–45	–70	754	644	642	588	166
Low	0.0001	0.0001	0.0041	528	–83	–100	680	598	596	507	143
High	0.054	0.0167	0.0249	732	20	–16	765	680	650	588	220
Range	0.0539	0.0166	0.0208	204	103	84	85	82	54	81	77

*The transformation temperature for weld V1 obtained from graphical interpolation of the curve shown in Fig. 7.

at 67 ppm (0.0067 wt-%) N content and 48 ppm (0.0048 wt-%) B content. In comparison, weld Z2 contained 230 ppm (0.023 wt-%) N but almost the same level of Ti, B, Al, and O additions as in weld Z, indicating that N addition at more than 100 ppm or 0.01 wt-% is deleterious to CVN impact toughness.

Table 3 shows selected CMCs of the 13 TiBAlN series of WMs. As C, Mn, and Si contents varied over a narrow range and the rest of the principal alloy elements were essentially held constant, the CMCs didn't show significant differences. In particular, the calculated A_{r3} temperature showed a narrow range, between 751° and 774°C. The O2 weld with 399 ppm (0.0399 wt-%) O and 235 ppm (0.0235 wt-%) N showed the lowest calculated A_{r3} temperature at 751°C. Both welds Y and Z showed a calculated A_{r3} temperature of 760°C, midway in the 751°–774°C range.

Table 4 shows the absorbed energy of CVN test results of the 13 TiBAlN series of welds. Actual test temperatures ranged from –120° to +40°C (Ref. 25). Figure 3 shows a plot of CVN absorbed energy values (in Joules) against test temperatures.

Weld Z showed the best CVN impact toughness behavior, with high upper shelf energy and the lowest ductile-to-brittle transition temperature, followed by weld X. Considering that welds Z and Y showed a lower calculated A_{r3} temperature, minimal N content, and excellent CVN impact toughness, one could consider welds Y and Z as offering the most desirable baselines for the selection of WM compositions with Ti-B-Al-O-N additions. Weld Z contained Ti at 420 ppm (0.042 wt-%), B at 48 ppm (0.0048 wt-%), O at 438 ppm (0.0438 wt-%), Al at 160 ppm (0.016 wt-%), and N at 67 ppm (0.0067 wt-%). One might notice that in weld Z, the N content was at the low end of the range while the Al content was at the intermediate range used in building the TiBAlN series of welds (Fig. 2).

While considering Ti-B-Al-O-N additions, it may be wiser to avoid both the rich and lean ends for all these alloy elements except N, which should be held at the lean end, preferably much below 80 ppm (0.0080 wt-%). Similarly, excessive Al additions over 500 ppm (0.05 wt-%), as in welds V, V1, and V2, could potentially result in free Al in solution that could seriously harm fracture toughness. Furthermore, considering the need for effective deoxidation and denitrogenation, particularly when both O and N contents remain high, as in welds V1 and V2, it may be necessary to ensure adequate additions of Ti and Al to tie up O, besides additions of B and Al to tie up N. Here, Ti addition is known to protect B from oxidation while allowing B to preferentially react with N, thus reducing free nitrogen in solution. Furthermore, soluble B is known to preferentially segregate to prior austenite grain boundaries

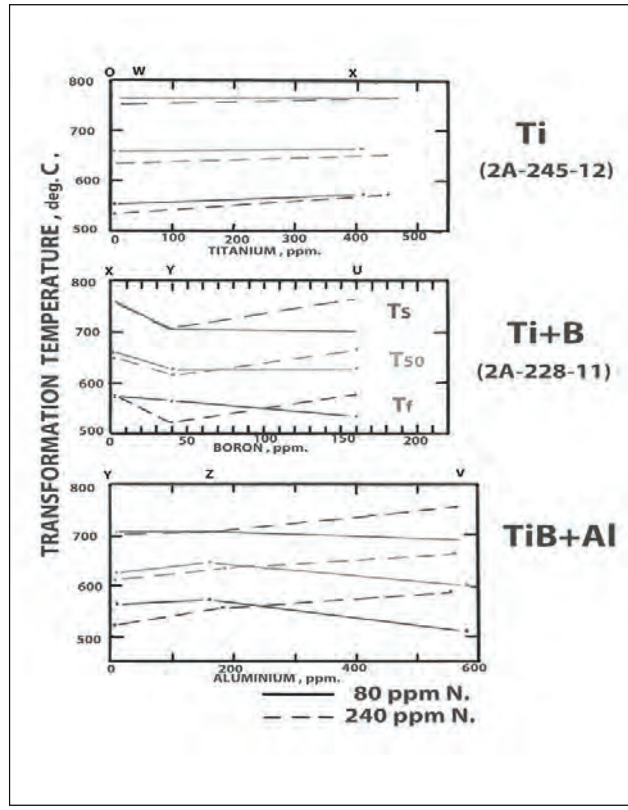

Fig. 9 — A summary of the effects of Ti, B, and Al additions on transformation temperatures (Ref. 25).

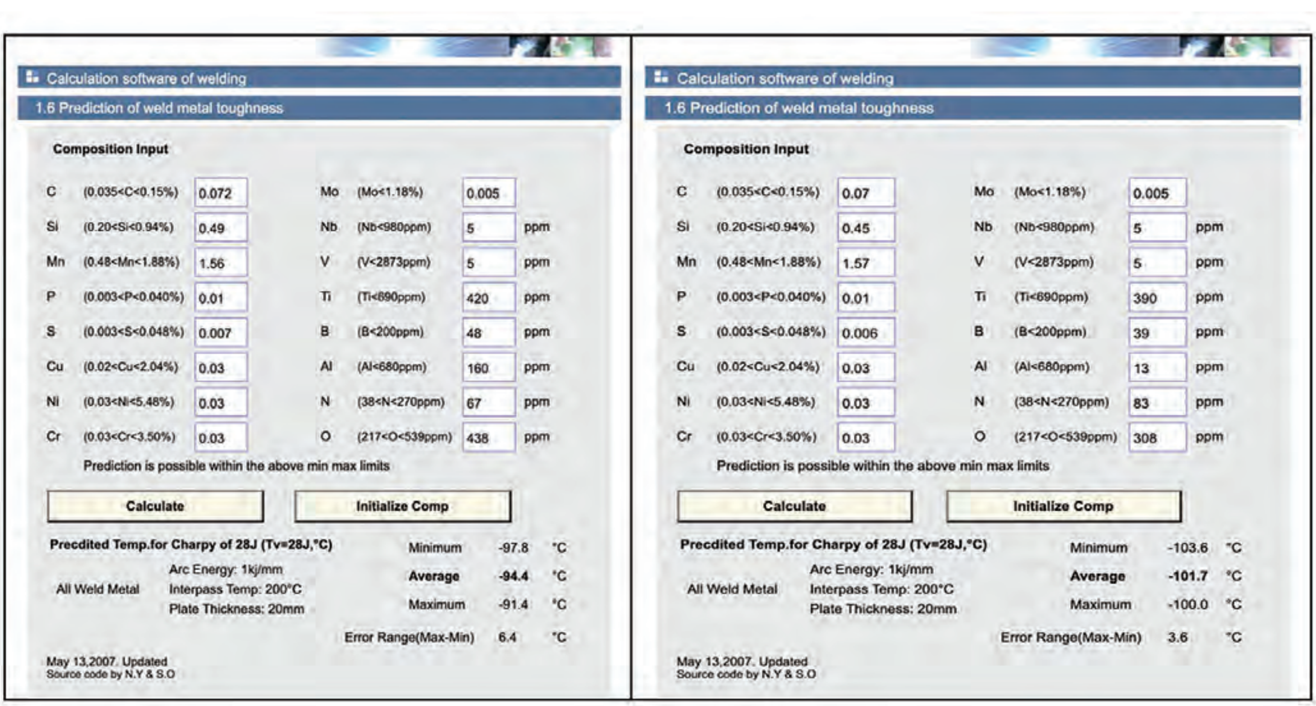

Fig. 10 — The JWES neural network predicted temperatures for 28 J absorbed energy for welds Z and Y.

Table 6 — Dilatometric and Calculated Transformation Temperatures of 13 TiBAlN Welds (Refs. 26–28)

Weld ID	Ti Content (wt-%)	B Content (wt-%)	Al Content (wt-%)	N Content (wt-%)	UTS (MPa)	Transformation Temperature (°C)	
						T_s (Dilatometry)	A_{r3} (Calculated)
O	0.0001	0.0001	0.0006	0.0079	528	762	772
O2	0.0005	0.0005	0.0005	0.0235	607	754	751
X	0.041	0.0002	0.0001	0.0077	577	760	768
X2	0.045	0.0002	0.0005	0.0249	631	760	769
Y	0.039	0.0039	0.0013	0.0083	594	710	760
Y2	0.041	0.0044	0.0005	0.0232	605	703	765
Z	0.042	0.0048	0.016	0.0067	640	710	760
Z2	0.047	0.0045	0.018	0.023	583	703	770
U	0.039	0.0158	0.0005	0.0084	586	700	770
U2	0.039	0.0167	0.0005	0.0217	541	765	763
V	0.054	0.0056	0.058	0.0041	732	680	768
V1	0.048	0.0044	0.056	0.012	644	760	771
V2	0.043	0.0035	0.056	0.0235	591	754	772
Low	0.0001	0.0001	0.0001	0.0041	528	680	751
High	0.054	0.0167	0.058	0.0249	732	765	772
Range	0.0539	0.0166	0.0579	0.0208	204	85	21

and retard the nucleation of grain boundary ferrite during austenite-to-ferrite transformation.

As is well known, Al is a strong deoxidizer. When the Al content is typically below 160 ppm (0.016 wt-%), as in welds Y and Z together with Ti, Al tends to form Al_2O_3 inclusions with a TiO layer. The Al_2O_3 inclusions with TiO layers serve as effective sites for the heterogeneous nucleation of acicular ferrite and promote intragranular nucleation of acicular ferrite (Ref. 29). Crystallographic orientations that provide a minimal lattice disregistry between inclusions and ferrite are quite effective in nucleating acicular ferrite. For example, inclusions, such as Al_2O_3 , $MnO.Al_2O_3$, TiN, and TiO, all appear to be effective at epitaxial growth of acicular ferrite in Fe-C-Mn steel WM. However, when soluble Al in the Ti-B WMs is about 580 ppm (0.058 wt-%), as in weld V, Al appears to retard the transformation of austenite to ferrite, leading to the formation of a bainitic microstructure in WM.

Dilatometric Evaluation

Figures 4–7 show fraction austenite that transformed to ferrite vs. transformation temperature for the 13 (O, O2, X, X2, Y, Y2, Z, Z2, U, U2, V, V1, and V2) welds. As seen in Fig. 6, between 0.2 and 0.8 fraction ferrite, the dilatometric curves for welds V2, Z, and Z2 showed a steeper gradient. This steeper gradient is associated with intragranular nucleation and growth of acicular ferrite aided by the presence of a large amount of microalloy additions. Weld Z2 showed the lowest difference between T_s and T_f temperatures at 143°C. Weld Y showed a 150°C difference, while weld Z showed a

Table 7 — Actual Test Results and Predicted Results of CVN Temperature for 28 J Absorbed Energy (Refs. 26–28)

Weld ID	Ti Content (wt-%)	B Content (wt-%)	Al Content (wt-%)	N Content (wt-%)	UTS (MPa)	CVN Actual Test Temperature (°C) @ 28 J	CVN Predicted Temperature (°C) @ 28 J
O	0.0001	0.0001	0.0006	0.0079	528	–42	–49
O2	0.0005	0.0005	0.0005	0.0235	607	–16	–15
X	0.041	0.0002	0.0001	0.0077	577	–77	–80
X2	0.045	0.0002	0.0005	0.0249	631	–58	–59
Y	0.039	0.0039	0.0013	0.0083	594	–98	–102
Y2	0.041	0.0044	0.0005	0.0232	605	–56	–54
Z	0.042	0.0048	0.016	0.0067	640	–100	–94
Z2	0.047	0.0045	0.018	0.023	583	–18	–28
U	0.039	0.0158	0.0005	0.0084	586	–80	–79
U2	0.039	0.0167	0.0005	0.0217	541	–81	–78
V	0.054	0.0056	0.058	0.0041	732	–46	–47
V1	0.048	0.0044	0.056	0.012	644	–93	–93
V2	0.043	0.0035	0.056	0.0235	591	–70	–71
Low	0.0001	0.0001	0.0001	0.0041	528	–100	–102
High	0.054	0.0167	0.058	0.0249	732	–16	–15
Range	0.0539	0.0166	0.0579	0.0208	204	84	87

160°C difference for T_s–T_f. As welds Y and Z showed a lower N content, a combination of other microalloy additions provided a balance that was perhaps quite effective in producing a larger increase in the volume fraction of evenly dispersed inclusions that likely aided the formation of acicular ferrite microstructure over a narrow T_s–T_f temperature range. In addition to a low N content, both a lower T_s temperature and a narrow T_s–T_f temperature range appeared helpful in achieving exceptional CVN impact toughness.

Table 5 shows the numerical values for the various transformation temperatures, along with UTS and CVN test temperatures for 100 and 28 J absorbed energy of the 13 welds (Refs. 26–28). Weld V had the lowest T_s temperature at 680°C and correspondingly the highest UTS at 732 MPa. A progressive increase in T_s temperature occurred from welds U, Y2, Z2, Y, Z, O2, V2, X, X2, V1, O, and U2. Correspondingly, a progressive decrease in UTS from 644 to 528 MPa occurred in welds V1, Z, X2, O2, Y2, Y, V2, U, Z2, X, U2, and O. When weld metal N content is below 80 ppm (0.008 wt-%), the overall trend between T_s temperature and UTS among all six welds is found to be highly correlated, as shown in Fig. 8. Two of these six welds, welds Z (with 640 MPa UTS) and Y (with 594 MPa UTS), appeared closer and on either side of the trend line, indicating that their Ti, B, Al, O, and N additions are well or adequately balanced. The trendline clearly confirmed the metallurgical principle that lowering the transformation temperature helped increase WM tensile strength. The trendline also indicated that a transformation temperature much below 680°C appeared essential to achieving a WM tensile strength more than 700 MPa (100 ksi).

Table 8 — Chemical Composition of Eight Fe-C-Mn Welds (Refs. 21, 22)

Weld Alloy Type	Weld Metal Chemical Composition (wt-%)											
	C	Mn	P	S	Si	Cr	Ni	Mo	V	Nb	Cu	Ti
Y	0.07	1.57	0.01	0.006	0.45	0.03	0.03	0.005	0.0005	0.0005	0.03	0.039
CB	0.075	1.5	0.01	0.006	0.4	0.03	0.03	0.005	0.0005	0.0005	0.03	0.039
CB	0.075	1.49	0.01	0.006	0.37	0.03	0.03	0.005	0.0005	0.0005	0.03	0.037
TiOX	0.085	1.63	0.01	0.004	0.34	0.03	0.03	0.005	0.0005	0.0005	0.03	0.0025
CB	0.073	1.54	0.01	0.006	0.48	0.03	0.03	0.005	0.0005	0.0005	0.03	0.052
TiBN	0.079	1.54	0.01	0.006	0.48	0.03	0.03	0.005	0.0005	0.0005	0.03	0.061
Z	0.072	1.56	0.01	0.007	0.49	0.03	0.03	0.005	0.0005	0.0005	0.03	0.042
CB	0.074	1.5	0.009	0.006	0.39	0.03	0.03	0.005	0.0005	0.0005	0.03	0.041
Low	0.07	1.49	0.009	0.004	0.34	0.03	0.03	0.005	0.0005	0.0005	0.03	0.0025
High	0.085	1.63	0.01	0.007	0.49	0.03	0.03	0.005	0.0005	0.0005	0.03	0.061
Range	0.015	0.14	0.001	0.003	0.15	0	0	0	0	0	0	0.0585

However, a direct correlation of transformation temperature with test temperatures for 100 and 28 J CVN absorbed energy didn't readily offer a clear trend. Lower shelf energy is generally controlled by microstructural features, while upper shelf energy is controlled mostly by the presence of inclusions and second phase particles that form cup and cone features during fracture, showing ductile dimples. Weld Z had the lowest test temperature at –83°C for 100 J absorbed energy and –100°C for 28 J absorbed energy, followed by welds Y, X, U, U2, V2, Y2, V, and Z2. Of the 13 welds, the Z2 and Z welds showed the temperature for 100 J absorbed energy transitioning from +13° to –83°C, indicating that a high N addition in the Z2 weld was not clearly advantageous. However, the lower CVN test temperatures for 100 and 28 J absorbed energy of the V1 and V2 welds indicated that a higher N content can be tolerated when the N content is effectively tied up with a higher B content and a higher Al content (Ref. 27). Incidentally, as shown in Table 6 for the U2 weld, a comparison of the experimentally determined T_s temperature at 765°C and the calculated A_{r3} temperature at 763°C indicated a marginally higher T_s temperature, meaning N addition seemed to nullify the beneficial effects of Ti, B, Al, and O additions in substantially lowering the T_s temperature, as opposed to welds U, Y, and Z, wherein the respective T_s temperature was substantially lower than the corresponding calculated A_{r3} temperature. Although weld V showed the largest difference between T_s temperature and calculated A_{r3} temperature and a low N content at 41 ppm (0.0041 wt-%), an excessive Ti content at 540 ppm (0.054 wt-%) likely resulted in a lower CVN impact toughness.

Figure 9 shows a summary of the research results (Ref. 25), revealing that increasing the Ti content at the lowest N level had virtually no effect on experimentally determined T_s and T_f temperatures.

CVN Impact Temperature Prediction

At the JWES website, one can calculate and predict the temperature for 28 J CVN impact toughness or the absorbed energy of Fe-C-Mn WMs based on their chemical composition, with certain minimum and maximum limits for specific elements. The prediction is performed using neural network analysis by a software developed by D. J. C. MacKay at the University of Cambridge. The prediction is possible within the minimum and maximum limits for specific elements, and the prediction uses the large SMAW database developed at Oerlikon Welding Ltd., on low alloy high-strength steel WM as a basis, and this database (Refs. 21, 22) has been made available to the University of Cambridge (*msm.cam.ac.uk/map/data/materials*). The database contains properties of all weld metals obtained under a constant welding condition of 1 kJ/mm arc energy, 200°C interpass temperature, and 20 mm plate thickness. The neural network prediction gives

Table 8 — (continued)

Weld Alloy Type	Weld Metal Chemical Composition (wt-%)			
	B	O	Al	N
Y	0.0039	0.0308	0.0013	0.0083
CB	0.0051	0.0297	0.0005	0.0085
CB	0.0041	0.0282	0.0005	0.0069
TiOX	0.0002	0.0276	0.0005	0.0068
CB	0.0032	0.0294	0.0005	0.0084
TiBN	0.0014	0.0276	0.0005	0.0081
Z	0.0048	0.0438	0.016	0.0067
CB	0.0029	0.0275	0.0005	0.0072
Low	0.0002	0.0275	0.0005	0.0067
High	0.0051	0.0438	0.016	0.0085
Range	0.0049	0.0163	0.0155	0.0018

Table 9 — Tensile and CVN Impact Properties of Eight Fe-C-Mn Welds (Refs. 21, 22)

Weld Alloy Type	Weld Metal Tensile Properties				CVN Test Temperature (°C)	
	YS (MPa)	UTS (MPa)	El (%)	RA (%)	@ 100 J	@ 28 J
Y	546	594	25.8	73	−84	−114
CB	514	571	28	79	−83	−108
CB	546	594	25.8	73	−81	−107
TiOX	489	560	26.8	80.7	−84	−106
CB	516	590	26.2	75	−76	−103
TiBN	545	617	25.4	76.9	−74	−100
Z	610	640	27.2	73.4	−83	−100
CB	548	590	25.4	75	−79	−100
Low	489	560	25.4	73	−84	−114
High	610	640	28	80.7	−74	−100
Range	121	80	2.6	7.7	10	14

maximum, minimum, and average values of temperature for 28 J CVN impact toughness or absorbed energy along with the degree of prediction error. When the difference between the maximum and minimum predicted values is over 30°C, the prediction is considered unreliable.

Table 7 shows a comparison of the actual test values and predicted results of CVN temperatures for 28 J absorbed energy for the 13 welds. The predicted values for the 13 welds were quite consistent with the actual test results in both values and trend, and the error values associated with predictions were much less than 30°C for each of these welds. Figure 10 shows the predicted temperatures for 28 J absorbed energy for welds Z and Y.

Discussion

Previous research on SMA WMs found that Ti addition provides a unique effect on the microstructure and properties of ferritic steel SMA WMs when a balance is achieved with other elements (B, Al, O, and N) present, leading to two optima, one at 30 ppm (0.003 wt-%) and the other at 180 to 400 ppm (0.018 to 0.04 wt-%) Ti content (Refs. 7, 8). The CVN impact toughness of SMA WMs containing either of the two optima remained robust across a range of weld cooling rates (Ref. 30). This behavior was attributed to the heterogenous nucleation and/or epitaxial growth of predominantly intragranular acicular ferrite microstructure. This is further supported by the steep gradient in the dilatometric results shown in Fig. 6.

Titanium is known to form a variety of oxides, such as TiO, Ti_2O_3, Ti_3O_5, and TiO_2. Of these oxides, TiO has the lowest Gibbs free energy (ΔG), therefore TiO is most likely to form a stable oxide. The TiO and/or Al_2O_3.TiO inclusions (Ref. 27), and occasionally TiN (Ref. 27) inclusions, appear to serve as effective sites for the intragranular nucleation of acicular ferrite, notably when the actual T_s temperature is 710°C or below.

Nitrogen addition at more than 80 ppm (0.008 wt-%) is generally considered deleterious to WM CVN impact toughness. However, it could be turned beneficial (Refs. 26–28) when B at about 40 ppm (0.004 wt-%) and Ti at about 400 ppm (0.04 wt-%) are added. In support, as shown in Fig. 7, a comparative dilatometric evaluation of transformation kinetics of welds V2, V1, and V showed that balancing N content vs. B and Ti contents retarded the T_s temperature associated with the formation of grain boundary ferrite in welds V1 and V2, further enabling the formation of a refined WM microstructure with predominantly acicular ferrite (Ref. 28) and improved CVN impact toughness compared to weld V (Table 5).

Table 10 — Selected CMCs of Eight Fe-C-Mn WMs with –100°C Cutoff for 28 J Absorbed Energy

Weld Alloy Type	Selected CMCs							
	P_{cm}	CE_{IIW}	CEN	A_{r3} (°C)	B_s (°C)	B_{50} (°C)	B_f (°C)	M_s (°C)
Y	0.187	0.418	0.244	760	666	606	546	475
CB	0.193	0.403	0.248	764	671	611	551	475
CB	0.186	0.396	0.243	764	672	612	552	475
TiOX	0.183	0.424	0.263	750	657	597	537	466
CB	0.186	0.421	0.245	761	668	608	548	474
TiBN	0.183	0.427	0.250	759	666	606	546	472
Z	0.194	0.425	0.250	760	667	607	547	474
CB	0.180	0.400	0.240	764	671	611	551	475
Low	0.180	0.396	0.240	750	657	597	537	466
High	0.194	0.427	0.263	764	672	612	552	475
Range	0.014	0.31	0.023	14	15	15	15	9

The comparative dilatometric experimental observations of reheated WM attest to the finding that one could reduce relevant transformation temperatures using a dual approach. In the first part of the dual approach, the contents of principal alloy elements, such as C, Mn, Ni, Cr, Mo, and Cu, are manipulated to achieve a target calculated A_{r3} transformation temperature range of 750° ± 10°C. As the constitutive equations for transformation temperatures make no reference to Ti-B-Al-N microalloying additions, in the second part of the dual approach, balanced amounts of Ti, B, Al, O, and N are added to further suppress the T_s temperature by another 60°C, thereby ensuring the development of a highly fracture resistant microstructure in WMs. Furthermore, the results of dilatometric experiments revealed the Ti-B-Al-O-N additions to offer nearly a 100°C shift in lowering the CVN test temperature for either 28 or 100 J absorbed energy. The present review illustrates the benefits of this dual approach, as balanced additions of Ti, B, Al, O, and N present in a series of TiBAlN WMs provided an exceptional combination of superior tensile and CVN impact properties.

Validation Testing

The above findings are supported by the results of dilatometric evaluation. However, in the absence of results on dilatometric evaluations of additional WMs, how could further validation testing be performed to ascertain various metallurgical design rules for welding electrode development for high performance applications?

Spreadsheet #4 shows a set of eight WMs that contained lower than 100 ppm (0.01 wt-%) N with a calculated A_{r3} temperature in a tight range of 750° to 764°C obtained from the large SMAW database, Spreadsheet #1 (Refs. 21, 22). Table 8 shows the chemical composition of this set of eight welds belonging to different types of Fe-C-Mn alloy systems that

Table 10 — (continued)

Weld Alloy Type	Selected CMCs			
	$(B_f–M_s)$ (°C)	$(A_{r3}–B_s)$ (°C)	$(A_{r3}–B_{50})$ (°C)	$(A_{r3}–B_f)$ (°C)
Y	71	93	153	213
CB	76	93	153	213
CB	77	92	152	212
TiOX	71	93	153	213
CB	74	93	153	213
TiBN	75	93	153	213
Z	72	93	153	213
CB	76	93	153	213
Low	71	92	152	212
High	77	93	153	213
Range	6	1	1	1

also included welds Y and Z. These eight welds showed a C content less than 0.10 wt-%, Mn between 1.49 and 1.63 wt-%, and a range of Ti, B, Al, and O contents. Table 9 shows WM tensile properties and CVN impact toughness test temperatures that achieved 100 and 28 J absorbed energy. The UTSs of these eight welds varied between 560 and 640 MPa, while the test temperatures for 28 J CVN absorbed energy varied between –114° and –100°C, and the test temperatures for 100 J CVN absorbed energy varied between –84° and –74°C. Table 10 shows the CMCs of these eight welds. Interestingly, the WM CEN values stayed well below 0.300 (at 0.263 maximum) while the calculated A_{r3} temperature occurred in a narrow range between 750° and 764°C. The calculated transformation temperatures of all eight WMs followed the common progression wherein $A_{r3} > B_s > B_f > M_s$. Results shown in Tables 8–10 further confirm that balanced additions of Ti, B, Al, and O, when N content is held below 0.085 wt-% in these eight Fe-C-Mn high-strength steel welds, provided an exceptional combination of superior tensile and CVN impact properties.

As shown in Spreadsheet #5, the manipulation of the large SMAW database while keeping the N content below 100 ppm (0.01 wt-%) but with the CVN test temperature for 28 J absorbed energy at –68°C as cutoff and relaxing the calculated A_{r3} temperature range revealed a total of 153 Fe-C-Mn WM compositions. Out of these 153 WMs, only one WM (Spreadsheet #5, Row #88, AlO) showed a high C content at 0.103 wt-%, while all other 152 WMs showed a C content less than 0.01 wt-%. As shown in Table 11, the calculated A_{r3} temperatures showed a wider range between 651°and 838°C and the calculated transformation temperatures of all 153 welds followed the common progression wherein $A_{r3} > B_s > B_f > M_s$. As shown in Spreadsheet #5, it appeared that Cu, Nb (Cb), and V additions aided in enlarging the total number of Fe-C-Mn WM compositions. Table 11 shows the low, high, and range of C, Mn, Ni, Ti, B, O, Al, and N contents; CEN and A_{r3} temperatures; and WM UTS and CVN test temperatures for 28 J absorbed energy with a –68°C cutoff.

When the above conditions were changed to a CVN test temperature for 28 J absorbed energy with a –92°C cutoff, the total number of Fe-C-Mn WM compositions dropped to 39, and the calculated A_{r3} temperature range narrowed between 669° and 781°C, as shown in Spreadsheet #6 and summarized in Table 12. The calculated transformation temperatures of all 39 welds followed the common progression wherein $A_{r3} > B_s > B_f > M_s$. In comparison with the 153 WM compositions shown in Spreadsheet #5, Cu, Nb (Cb), and V additions remained constant in the 39 WM compositions as shown in Spreadsheet #6. Table 12 shows the corresponding low, high, and range of C, Mn, Ni, Ti, B, O, Al, and N contents; CEN and A_{r3} temperatures; and WM UTS and CVN test temperatures for 28 J absorbed energy with a –92°C cutoff.

Conclusions

This review of selected dilatometric analyses of Fe-C-Mn high-strength steel WMs containing Ti, B, Al, O, and N additions offers the following metallurgical design rules on the development of high-strength, high-performance welding electrodes:

1) The electrode/WM design can be based on the metallurgical principle that lowering the austenite decomposition temperatures (primarily A_{r3}) improves both WM strength and fracture toughness, while simultaneously reducing carbon content and CEN improves weldability. Keeping C below 0.01 wt-% and CEN below 0.300 is adequate when designing WMs with about 700 MPa UTS.

2) Using the set of constitutive equations, one could control the amounts of principal alloy elements, so the calculated A_{r3} temperature stays in the range 750° ± 10°C. One also needs to ascertain that the common progression of calculated transformation temperatures, wherein $A_{r3} > B_s > B_f > M_s$, remains valid.

3) The Ti, B, Al, O, and N alloy additions need to closely match or achieve the following aim levels for composition control: Ti at 400 ppm (0.04 wt-%), B at 40 ppm (0.004 wt-%), Al at 200 ppm (0.020 wt-%), O at 400 ppm (0.04 wt-%), and N preferably below 80 ppm (0.008 wt-%) to achieve effective

Table 11 — Selected Values of 153 Fe-C-Mn WMs with −68°C Cutoff for 28 J Absorbed Energy

	C	Mn	Ni	Ti	B	O	Al	N	CEN	Calculated A_{r3} (°C)	UTS (MPa)	CVN Test Temperature (°C) for 28 J Absorbed Energy
Low	0.038	0.57	0.03	0.0002	0.0002	0.0217	0.0001	0.0041	0.138	651	452	−114
High	0.103	1.82	3.49	0.061	0.014	0.0528	0.034	0.0099	0.289	838	681	−68
Range	0.065	1.25	3.46	0.0608	0.0138	0.0311	0.0339	0.0058	0.1515	187	229	46

Table 12 — Selected Values of 39 Fe-C-Mn WMs with −92°C Cutoff for 28 J Absorbed Energy

	C	Mn	Ni	Ti	B	O	Al	N	CEN	Calculated A_{r3} (°C)	UTS (MPa)	CVN Test Temperature (°C) for 28 J Absorbed Energy
Low	0.057	0.57	0.03	0.0019	0.0002	0.024	0.0004	0.0043	0.189	669	524	−114
High	0.094	1.64	3.03	0.061	0.0091	0.046	0.017	0.0085	0.263	781	640	−92
Range	0.037	1.07	3.0	0.0591	0.0089	0.022	0.0166	0.0042	0.074	112	116	22

deoxidation, form complex inclusions, and distribute them to enable development of a fracture-resistant refined WM microstructure. The combined Ti, B, Al, O, and N additions offered nearly a 100°C shift in lowering the CVN test temperature for either 28 or 100 J absorbed energy.

4) The neural network template provided by the JWES at its website allows one to ascertain the predictive temperature range for achieving 28 J absorbed energy in CVN testing using selected WM compositions.

5) Dilatometric evaluations of reheated WMs show a) the balanced Ti, B, Al, O, and N additions lowered the actual T_s temperature by about 60°C compared to the calculated A_{r3} transformation temperature; b) both a lower T_s temperature and a narrow start-to-finish (T_s–T_f) temperature range appeared helpful or necessary in achieving exceptional CVN impact toughness; and c) N more than 100 ppm (0.010 wt-%) effectively nullified the beneficial effects of Ti, B, and Al additions in lowering the austenite transformation temperature.

Acknowledgments

The author remains grateful to Dr. Glyn M. Evans for his encouragement, technical guidance, and support. The author is quite thankful to the AWS peer reviewers for their insightful comments on the manuscript that enabled the author to further improve the organization, methodology, and readability of the manuscript.

References

1. Bailey, N., and Wright, M. D. 1993. Weldability of high strength steels. *Welding and Metal Fabrication* 61(8): 389-396.

2. Evans, G. M. 1983. Effect of carbon on the microstructure and properties of C-Mn all-weld metal deposits. *Welding Journal* 62(11): 313-s to 320-s.

3. Evans, G. M. 1980. Effect of manganese on the microstructure and properties of all-weld-metal deposits. *Welding Journal* 59(3): 67-s to 75-s.

4. Evans, G. M. 1986. Effect of silicon on the microstructure and properties of C-Mn all-weld-metal deposits. *Metal Construction* 18(7): 438R–444R.

5. Evans, G. M. 1988. Effect of molybdenum on microstructure and properties of C-Mn all-weld metal deposits. *Joining & Materials* 1(5): 239–246.

6. Evans, G. M. 1993. The effect of micro-alloying elements in C-Mn steel weld metals. *Welding in the World* 31(1): 12–19. DOI: 10.13140/RG.2.1.3253.9041

7. Evans, G. M. 1995. Microstructure and properties of ferritic steel welds containing Al and Ti. *Welding Journal* 74(8): 249-s to 261-s.

8. Evans, G. M. 1996. Microstructure and properties of ferritic steel welds containing Ti and B. *Welding Journal* 75(8): 251-s to 260-s.

9. Ito, Y., and Bessyo, K. 1968. *Weldability Formula of High Strength Steels Related to Heat Affected Zone Cracking*. International Institute of Welding. IIW Doc IX-576-68.

10. Dearden, J., and O'Neill, H. 1940. A guide to the selection and welding of low alloy structural steel. *Transactions of the Institute of Welding* 3: 203–214.

11. Yurioka, N., Suzuki, H., Ohshita, S., and Saito, S. 1983. Determination of necessary preheating temperature in steel welding. *Welding Journal* 62(6): 147-s to 153-s.

12. Ouchi, C., Sampei, T., and Kozasu, I. 1982. The effect of hot rolling condition and chemical composition on the onset temperature of γ-α transformation after hot rolling. *Transactions of the Iron and Steel Institute of Japan* 22(3): 214–222. DOI: 10.2355/isijinternational1966.22.214

13. Steven, W., and Haynes, A. G. 1956. The temperature of formation of martensite and bainite in low-alloy steels. *Journal of the Iron and Steel Institute* 183(8): 349–359.

14. Sampath, K. 2006. An understanding of HSLA-65 plate steels. *Journal of Materials Engineering and Performance* 15(1): 32–40. DOI: 10.1361/105994906x83439

15. Sampath, K. 2005. Constraints-based modeling enables successful development of a welding electrode specification for critical navy applications. *Welding Journal* 84(8): 131-s to 138-s.

16. Sampath, V., Kehl, J., Vizza, C., Varadan, R., and Sampath, K. 2008. Metallurgical design of high-performance GMAW electrodes for joining HSLA-65 steel. *Journal of Materials Engineering and Performance* 17(6): 808–830. DOI: 10.1007/s11665-008-9236-2

17. Lalam, S. H., Bhadeshia, H. K. D. H., and MacKay, D. J. C. 2000. Estimation of mechanical properties of ferritic steel welds. Part 1: Yield and tensile strength. *Science and Technology of Welding and Joining* 5(3): 135–147. DOI: 10.1179/136217100101538137

18. Lalam, S. H., Bhadeshia, H. K. D. H., and MacKay, D. J. C. 2000. Estimation of mechanical properties of ferritic steel welds. Part 2: Elongation and Charpy toughness. *Science and Technology of Welding and Joining* 5(3): 149-160. DOI: 10.1179/136217100101538146

19. Metzbower, E. A., DeLoach, J. J., Lalam, S. H., and Bhadeshia, H. K. D. H. 2001. Neural network analysis of strength and ductility of welding alloys for high strength low alloy shipbuilding steels. *Science and Technology of Welding and Joining* 6(2): 116–124. DOI: 10.1179/136217101101538622

20. Metzbower, E. A., DeLoach, J. J., Lalam, S. H., and Bhadeshia, H. K. D. H. 2001. Analysis of toughness of welding alloys for high strength low alloy shipbuilding steels. *Science and Technology of Welding and Joining* 6(6): 368–374. DOI: 10.1179/stw.2001.6.6.368

21. Evans, G. M., and Bailey, N. 1999. *Metallurgy of Basic Weld Metal*. Abington, UK: Abington Publishing.

22. Evans, G. M. 2015. Database — Weld metal composition and properties. DOI: 10.13140/RG.2.1.3628.1764

23. Evans, G. M. 2018. IIW Doc.II-C-546-18, A reassessment of the predictive Charpy-V toughness of the manganese-nickel weld metal combination. *IIW Intermediate Meeting Sub-Comm.IIC*, Genova, Italy.

24. Sampath, K. 2021. Analysis of a high-strength steel SMAW database. *Welding Journal* 100(12): 410-s to 420-s. DOI: 10.29391/2021.100.036

25. Evans, G. M. 2021. Private communication. 22 June 2021.

26. Ilman, M. N., Cochrane, R. C., and Evans, G. M. 2012. Effect of nitrogen and boron on the development of acicular ferrite in reheated C-Mn-Ti steel weld metals. *Welding in the World* 56: 41–50. DOI: 10.1007/BF03321394

27. Ilman, M. N., Cochrane, R. C., and Evans, G. M. 2014. Effect of titanium and nitrogen on the transformation characteristics of acicular ferrite in reheated C–Mn steel weld metals. *Welding in the World* 58: 1–10. DOI: 10.1007/s40194-013-0091-x

28. Ilman, M. N., Cochrane, R. C., and Evans, G. M. 2015. The development of acicular ferrite in reheated Ti-B-Al-N-type steel weld metals containing various levels of aluminium and nitrogen. *Welding in the World* 59: 565–575. DOI: 10.1007/s40194-015-0231-6

29. Fox, A. G., and Evans, G. M. 2013. A comparative study of the non-metallic inclusions in C-Mn steel weld metals containing titanium or aluminium. *Trends in Welding Research*. T. DebRoy, S. A. David, J. N. DuPont, T. Koseki, and H. K. Bhadeshia. ASM International, pp. 623–630.

30. Johnson, M. Q., Evans, G. M., and Edwards, G. R. 1995. The influence of titanium additions and interpass temperature on the microstructures and mechanical properties of high strength SMA weld metals. *ISIJ International* 35(10): 1222–1231. DOI: 10.2355/isijinternational.35.1222

K. SAMPATH (*krishna.sampath@icloud.com*) is with Creative Concepts, Marietta, Ga.